applied sciences

MDPI

Article

Combining Radon Deficit, NAPL Concentration, and Groundwater Table Dynamics to Assess Soil and Groundwater Contamination by NAPLs and Related Attenuation Processes

Martina Mattia [1], Paola Tuccimei [1,*], Giancarlo Ciotoli [2], Michele Soligo [1], Claudio Carusi [3], Elisa Rainaldi [3] and Mario Voltaggio [2]

[1] Dipartimento di Scienze, Università "Roma Tre", Largo San Leonardo Murialdo 1, 00146 Rome, Italy; michele.soligo@uniroma3.it (M.S.)
[2] Istituto di Geologia Ambientale e Geoingegneria, Consiglio Nazionale delle Ricerche, via Salaria km 29,300, 00146 Rome, Italy; giancarlo.ciotoli@cnr.it (G.C.)
[3] Protezione Ambiente, Mares S.r.L., via Fiume Giallo, 3, 00144 Rome, Italy; claudiocarusi@maresitalia.it (C.C.); elisarainaldi@maresitalia.it (E.R.)
* Correspondence: paola.tuccimei@uniroma3.it

Featured Application: Radon deficit reveals the presence of residual NAPL(Non-Aqueous Phase Liquid) contamination in soil and groundwater, giving a good picture of their vertical and spatial location. A combined and repeated approach consisting of measurements of radon and NAPL concentration coupled with groundwater table dynamics makes it possible to assess the evolution of the contamination phenomena. The application ofexploratory factor and principal component analyses to this dataset provides a key to understanding the attenuation processes, whether natural or induced, by the application of mitigation practices, and delivers models (conceptual and mathematical) to manage the site reclamation.

Abstract: Soil and groundwater contamination by NAPLs (Non-Aqueous Phase Liquids) is certainly a big issue for protecting the environment. In situ clean-up actions are routinely applied to mitigate the risk and are supplemented by monitoring surveys to assess the degree, extension, and evolution of the contamination. Radon gas is here used as a tracer of contamination because of its high solubility in non-polar solvents that produce a reduced concentration of the gas in polluted soil and groundwater with reference to radon levels in adjacent "clean" areas. This approach was employed in two sites where gasoline and diesel spillage occurred, causing soil and groundwater contamination. The two case studies were chosen because of their difference in terms of the hydrogeological features, age of the spillage, composition of residual NAPLs, and clean-up measures to test the advantages and limits of this approach in a variety of settings. Radon data, NAPL concentration in the groundwater (mainly total hydrocarbons, Methyl Tertiary-Butyl Ether and Ethyl Tertiary-Butyl Ether) and the depth of the groundwater table were periodically collected in surveys that spanned a period of two years. This dataset was statistically processed using principal component analysis to unravel which factors and attenuation processes are working in the sites and the response of the radon deficit approach to this complex series of phenomena concurrently occurring there.

Keywords: radon; NAPL; groundwater contamination; principal component analysis; Roma

Citation: Mattia, M.; Tuccimei, P.; Ciotoli, G.; Soligo, M.; Carusi, C.; Rainaldi, E.; Voltaggio, M. Combining Radon Deficit, NAPL Concentration, and Groundwater Table Dynamics to Assess Soil and Groundwater Contamination by NAPLs and Related Attenuation Processes. *Appl. Sci.* **2023**, *13*, 12813. https://doi.org/10.3390/app132312813

Academic Editor: Elida Nora Ferri

Received: 2 October 2023
Revised: 15 November 2023
Accepted: 21 November 2023
Published: 29 November 2023

1. Introduction

Non-Aqueous Phase Liquids, or NAPLs, are organic liquid contaminants that are poorly soluble in water such as oil, gasoline, and petroleum products. NAPLs tend to contaminate soil and groundwaters for very long periods of time and need to be removed with active (e.g., pump-and-treat, soil vapour extraction) or passive (natural attenuation)

remedial strategies [1]. The efficiency of both approaches relies on environmental monitoring [2] and on a suitable geochemical tracer of ongoing transport, dilution, degradation, and volatilization phenomena [3,4]. Radon gas can be used to identify NAPLs in soil and groundwater because of its preferential partitioning in organic phases [5–23]. The resulting radon deficit (regarding the site-specific radon background concentration in soil or groundwater) can be utilized as an NAPL indicator [17].

Moreover, it is possible to estimate the saturation of the residual NAPLs either in the vadose or saturated portion of an aquifer. NAPL saturation (S_{NAPL}) in the saturated aquifer, on top of the "NAPL source zone", or downgradient in the plume, can be calculated using the following equation [17]:

$$S_{NAPL}\ (\%) = [1 - \Delta C_\infty / (\Delta C_\infty \times K_{NAPL/W} - \Delta C_\infty)] \times 100 \quad (1)$$

where:

ΔC_∞: radon deficit = equilibrium radon concentration in NAPL polluted aquifer/equilibrium radon concentration in clean aquifer.

$K_{NAPL/W}$: radon partition coefficient between NAPL and water at Roma average temperature (70, [17,22])

It is worth noting that this equation, Equation (7) in ref [17], is affected by a typo in the numerator where "ΔS_∞" is reported in place of "ΔC_∞".

Although many works applied this approach to estimate the amount of the residual NAPLs in soil and groundwater (see for example, [8,17,24,25]), to our knowledge no references are available for a statistical treatment of radon and NAPL concentration, in terms of principal component analysis. This research is a first example of the potential of such a kind of approach to infer processes accounting for relationships among relevant parameters (radon, NAPLs, water table fluctuations) to successfully manage the reclamation of a contaminated area. Since groundwater monitoring and sampling is routinely carried out once every two–three months by companies responsible for remediation actions, it is particularly useful to have a tool to establish relations among variables and understand the evolution of contamination with standard sampling times.

Two study sites, with different hydrogeological features, age of the spillage, composition of residual NAPLs, and clean-up procedures are employed here to show the advantages and drawbacks of this method. The factor analysis is here applied only to groundwater and not soil variables' data, which were not available with the same frequency; however, the same approach can be extended to soil contamination in case of a larger dataset.

2. Study Areas

Two Areas in the City of Roma (Central Italy) Were Selected for This Study

Volcanic products from Colli Albani volcano are the geological bedrock of site 1 (Figure 1) and represent the local aquifer (Colli Albani hydrogeological unit [26]). The groundwater table, located at a depth of about 18 m, is characterized by high radon levels [23]. Small seasonal fluctuations affect the aquifer and groundwater flow direction is constant throughout the year. The gasoline spillage occurred about 20 years ago; a "Pump-and-Treat" system coupled with a set of Soil Vapor Extraction (SVE) wells (Figure 2) is employed here for in situ clean-up of soil and groundwater. Biosurfactants were also added to enhance the separation of the residual NAPLs from soil grains and the biodegradation.

Site 2, located next to Tevere river, is characterized by an alluvial bedrock (Figure 1). The groundwater table is very shallow (about 2 m below ground level) with significant seasonal fluctuation (up to 0.7 m) and changing flow direction throughout the year. Radon contents are from low to moderate. The NAPL (diesel) spillage is much more recent here (January 2019) compared to site 1, even if previous gasoline leakages were reported in the past. The age of the diesel spill was estimated applying a radiometric method, based on the $^{228}Th/^{228}Ra$ activity ratio in the NAPL phase extracted from the aquifer [27].

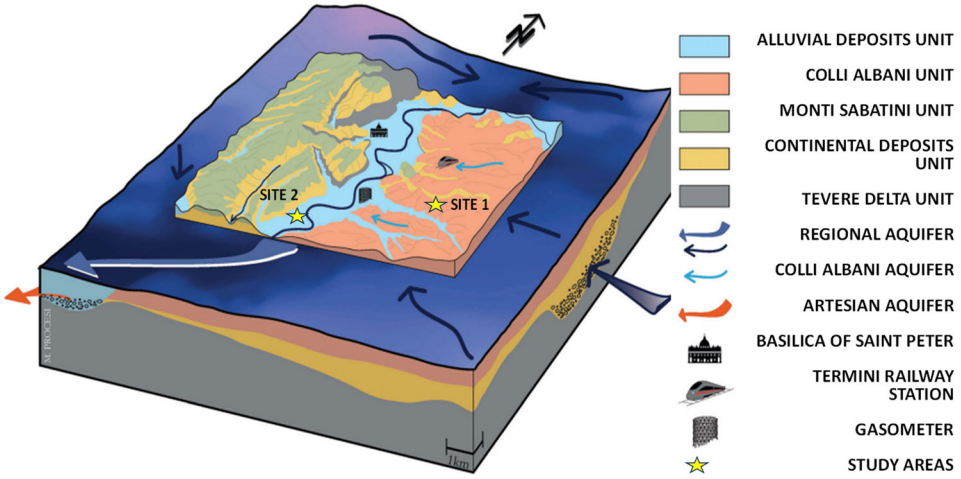

Figure 1. Hydrogeological conceptual model of Roma (central Italy) with location of the two study areas. Modified from [26].

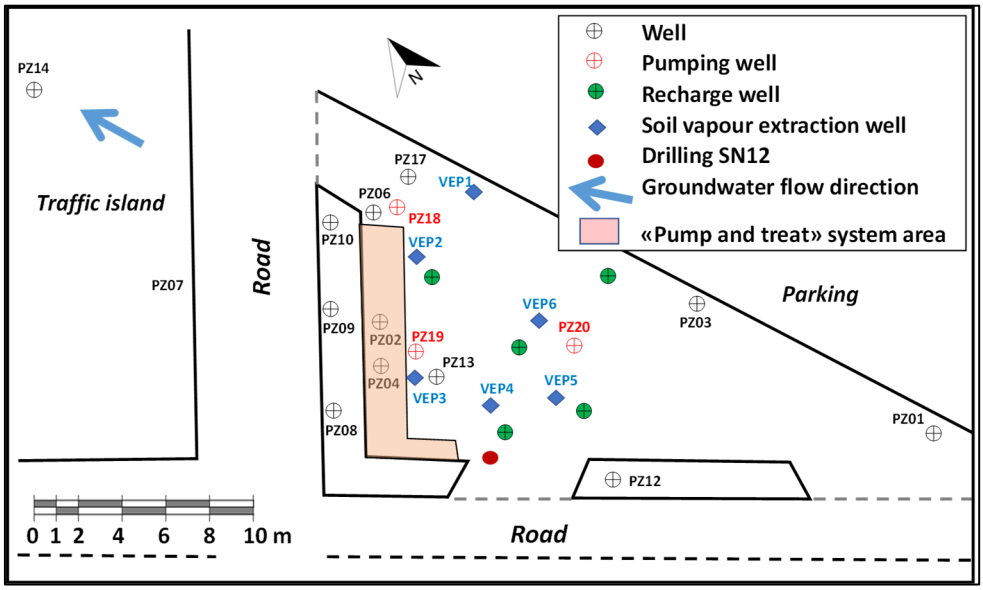

Figure 2. Site 1. The mitigation plant consists of a "Pump-and-Treat" system, coupled with a set of Soil Vapor Extraction (SVE) wells. Wells PZ25 and PZ26, located about 200 m E and SE of the petrol station area, are not reported in the map to avoid narrowing the petrol station area too much. Their location is provided in ref [23], Figure 3.

No mitigation actions have been taken so far, but securing activities such as monitoring, pumping, and local storage of extracted groundwater are operative (Figure 3).

In both areas, water sampling from purged wells is carried out every three months and the groundwater is analyzed for radon activity concentration and NAPL content, mainly total hydrocarbons, MTBE (Methyl Tertiary-Butyl Ether), and ETBE (Ethyl Tertiary-Butyl Ether). The depth of the groundwater table is measured once a week and occasionally soil gas is extracted for radon and volatile organic compounds (VOCs) detection.

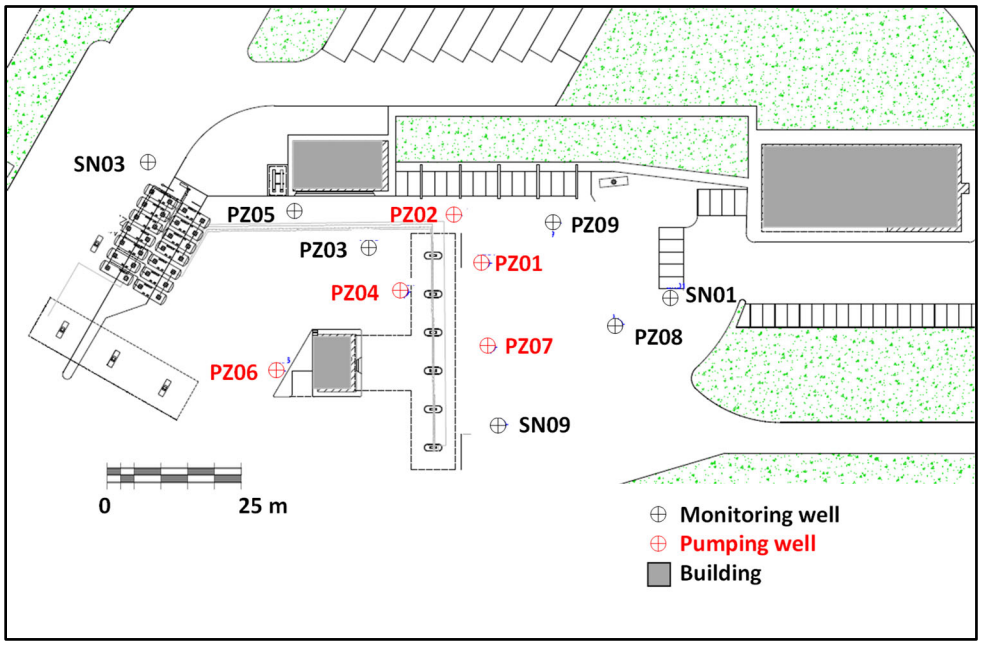

Figure 3. Remediation system at the study site 2. Wells PZ01, PZ02, PZ04, PZ06, and PZ07 are connected to a pumping system, working intermittently to guarantee that NAPLs are not dispersed.

3. Materials and Methods

3.1. Field Work

Two sites in Roma were selected based on their different hydrogeological features, age of the spillage, composition of residual NAPLs, and clean-up procedures to test the advantages and limits of this combined multiparameter approach.

3.1.1. Site 1

In the period 2020–2022, eighteen wells were monitored in site 1, fourteen in the petrol station area, and four in the adjacent clean area placed upgradient or to the side of the removed leaking underground tanks (Figure 2) [23]. In these campaigns, the groundwater level was measured, and water was sampled for radon and NAPL determinations.

After purging, soil gas was extracted thrice from two vapor extraction wells at different depths (0–5, 6–10, 11–14, 15–18 m) to measure the methane and radon concentration using a pump and modified Marinelli beakers with two taps on the upper lid. Methane was detected in situ using a multi-gas detector (Dräger X-AM 7000, Drägerwerk AG & Co. KGaA, Lübeck, Germany).

A drilling, SN 12, was made in November 2020 to reconstruct the stratigraphy, detect any residual VOC concentration in the vadose zone, and collect samples for ^{226}Ra determination. The VOC levels were measured in the field using a photoionization detector (PID) employing an ultraviolet source to bombard gas samples and detect volatile substances.

3.1.2. Site 2

Twelve wells were monitored in site 2, either in the petrol station area or in the close adjacent clean zone in the period 2021–2022 (Figure 3). The groundwater level was always detected, and water samples were extracted for radon and NAPL determination. Three wells (SN1, SN3 and SN9) out of twelve (Figure 3) belonging to a previous monitoring network were cemented in April 2022 and not included in the latest sampling campaigns.

3.2. Laboratory Methods

Groundwater samples were investigated for radon and NAPL concentration.

Water samples were collected in 500 or 660 mL PET bottles to avoid radon loss during sample storage [28–30] and then analyzed using a RAD7 monitor (Durridge Company Inc.,

Billerica, MA, USA) equipped with the Big Bottle RAD H_2O accessory. This experimental set-up was extensively and thoroughly described in earlier studies [20,22,31]. It consists of several components: the PET bottle, the bubble trap, the aeration system, the temperature data logger, vinyl tubing with an aeration stone fixed at its lower end and a cap at the upper end, the laboratory dryer, and the RAD7. The experimental apparatus is shown in Figure 4 of [23]. Two cycles of 15 min each have been set for the analysis.

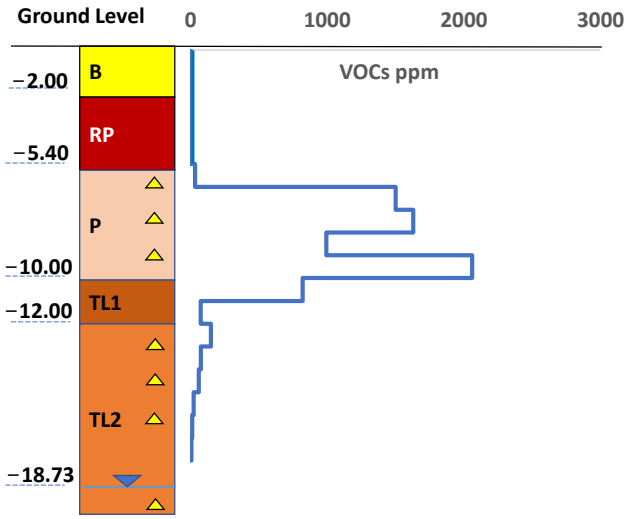

Figure 4. SN12 drilling with concentration of VOCs. B is Backfill; RP stands for Reworked Pozzolan; P is Pozzolanelle Unit; TL1 is Tufo Lionato Unit (lithoid facies) and TL2 Tufo Lionato Unit (granular facies). The yellow triangles are soil samples for ^{226}Ra determination.

Soil gas samples were pumped from the vapor extraction wells and stored in 500 mL Marinelli beakers, equipped with two taps on the upper lid (see also Section 3.1.1). Soil gas was then analyzed in the laboratory using the RAD7 monitor connected in a closed loop with the vessel via vinyl tubing. Two 30 min cycles were used, but the first was discarded because the radioactive equilibrium between radon and its daughter ^{218}Po is reached only after 15 min. Radon data were corrected for the effect water molecules on the efficiency of the silicon detector [28] and for decay between sampling and measurement, taking into account the volume of the Marinelli beaker and that of the experimental circuit.

NAPL concentrations were provided by MARES S.r.L.

^{226}Ra determination on soil samples from SN12 drilling in site 1 was carried out using gamma spectrometry. Samples of 400 gr were dried at 100 °C, placed in 500 mL Marinelli beaker, and analyzed with a lanthanum bromide detector (LaBr3(Ce), ORTEC-AMETEK, Oak Ridge, TN, USA) coupled with a photomultiplier (PMT Photonis XP5500, ORTEC-AMETEK), connected to a 1024-channel portable multichannel system (Digibase, ORTEC-AMETEK). The Marinelli beaker was introduced in a lead housing and counted for 2 h. Samples analyses were alternated with the measurements of the environmental background for correction. The 186 keV peak of ^{226}Ra and an ignimbrite standard (S6 from Caprarola area, Central Italy, [32]) were used for calculation.

3.3. Statistical Treatment

Radon concentrations in groundwater, water table depth, and NAPL contents (total hydrocarbon, MTBE and ETBE) in the two sites were statistically processed using principal component analysis. Processes such as radon preferential solubility in NAPLs, biodegradation of hydrocarbons mixtures in aerobic/anaerobic conditions, and volatilization were analyzed and evaluated as principal components to explain the maximum amount of variance. Data were processed using Minitab 2.0 (gmsl Minitab, LLC., State College, PA, USA), MedCalc 1.0 (MedCalc Software Ltd., Oostende, Belgium), and Stratgraphics 19.1 (1982–2020 by Statgraphics technologies, Inc. centurion, The Plains, VA, USA) softwares.

4. Results

4.1. Site 1

Table 1 shows the radon activity concentrations of the groundwater extracted from the 18 wells of site 1 in the period 2020–2022. Tables A1 and A2 report correspondent groundwater levels and contents of NAPLs (total hydrocarbons, MTBE, and ETBE), respectively.

Table 1. Radon activity concentrations in the 18 monitoring wells of site 1 in the period 2020–2022.

Wells	^{222}Rn (Bq L^{-1})	^{222}Rn (Bq L^{-1})	^{222}Rn (Bq L^{-1})	^{222}Rn (Bq L^{-1})	^{222}Rn (Bq L^{-1})	^{222}Rn (Bq L^{-1})	^{222}Rn (Bq L^{-1})	^{222}Rn (Bq L^{-1})
	February 2020	**May 2020**	**November 2020**	**February 2021**	**May 2021**	**July 2021**	**November 2021**	**April 2022**
PZ25	102 ± 7	86 ± 6	95 ± 6	77 ± 5	105 ± 7	102 ± 6	106 ± 7	49 ± 3
PZ26	125 ± 8	112 ± 7	119 ± 8	125 ± 8	139 9	130 ± 8	136 ± 8	133 ± 8
PZ7	87 ± 6	115 ± 7	108 ± 7	107 ± 7	124 ± 8	124 ± 8	116 ± 7	125 ± 8
PZ14	105 ± 7	180 ± 11	93 ± 6	102 ± 7	107 ± 7	89 ± 6	104 ± 7	104 ± 7
PZ01	158 ± 10	166 ± 10	116 ± 7	112 ± 7	115 ± 7	119 ± 8	135 ± 8	125 ± 8
PZ03	82 ± 5	132 ± 8	171 ± 11	160 ± 10	185 ± 11	168 ± 10	179 ± 11	167 ± 10
PZ12	106 ± 6	74 ± 5	81 ± 5	67 ± 4	88 ± 6	79 ± 5	101 ± 6	105 ± 7
PZ17	87 ± 6	104 ± 7	95 ± 6	95 ± 6	87 ± 6	73 ± 5	106 ± 7	113 ± 7
PZ06	118 ± 7	118 ± 6	96 ± 6	87 ± 6	95 ± 6	120 ± 8	101 ± 6	98 ± 6
PZ08	98 ± 6	70 ± 5	126 ± 8	76 ± 5	69 ± 4	101 ± 6	113 ± 7	127 ± 8
PZ09	60 ± 4	73 ± 5	79 ± 5	47 ± 3	68 ± 4	99 ± 6	103 ± 6	15 ± 9
PZ10	70 ± 5	100 ± 6	74 ± 5	43 ± 3	80 ± 5	70 ± 5	77 ± 5	70 ± 4
PZ04	72 ± 5	58 ± 4	60 ± 4	17 ± 1	43 ± 3	110 ± 7	79 ± 5	67 ± 4
PZ02	75 ± 5	63 ± 4	63 ± 4	42 ± 3	109 ± 7	41 ± 3	101 ± 6	114 ± 7
PZ18	90 ± 6	103 ± 7	81 ± 5	79 ± 5	105 ± 7	93 ± 6	115 ± 7	114 ± 7
PZ19	55 ± 4	81 ± 5	73 ± 5	80 ± 5	114 ± 7	138 ± 9	111 ± 7	113 ± 7
PZ20	95 ± 5	119 ± 8	104 ± 7	96 6	126 ± 8	112 ± 7	114 ± 7	128 ± 8
PZ13	61 ± 4	40 ± 3	38 ± 3	29 ± 2	43 ± 3	47 ± 3	59 ± 4	24 ± 2

Radon levels ranged from 17 Bq L^{-1} (well PZ04 in November 2020) to 185 Bq L^{-1} (well PZ03 in May 2021). Lower values were generally recorded in some wells within the study area (wells PZ02, PZ04, PZ08, PZ09, PZ10, PZ13, and PZ19, see Figure 2 for locations), adjacent to or downgradient of the removed leaking underground tank.

Higher radon concentrations, found in wells PZ03, PZ07, PZ14, PZ25, and PZ26 (see Figure 2 for locations) located away from the contamination, were used to calculate the average radon in the clean wells (119 ± 11 Bq L^{-1}); this value was then employed as a reference to estimate the radon deficit and the NAPL saturation of "dirty" wells.

Radon activity concentrations in soil gas extracted at different depths from vapor extraction wells 1 (VEP01) in December 2021 and vapor extraction well 4 (VEP04) in May and October 2021 are reported in Table 2. The location of VEP01 and VEP04 can be found in Figure 2. Table 2 also reports VOC and CH_4 concentration detected in situ during soil gas sampling. Low radon values (<1100 Bq m^{-3}) and/or high methane (up to 60,000 ppm) and VOC (up to 615 ppm) contents were detected at depths of 6–10 and 11–14 m, while no methane, negligible VOCs (never higher than 26 ppm), and relevant radon concentrations (up to 175,000 Bq m^{-3}) were found at depths of 0–5 and 15–18 m. This inverse correlation between radon and residual organic compounds agrees with the radon deficit rationale according to which radon remains trapped within the pure residual NAPLs producing a concentration deficit compared to nearby unpolluted soil areas.

Residual VOCs were detected in November 2020 on the cores of SN12 drilling (Figure 4). Highest levels were found between 6 and 13 m in agreement with methane and VOC data from VEP01 vapor extraction well in December 2021 (Table 2).

^{226}Ra specific activities of soil samples from SN12 drilling (Figure 4), measured by gamma spectrometry, are reported in Table A3. They range from 37 to 157 Bq kg $^{-1}$.

Table 2. Radon, methane, and VOC concentration in soil gas from two vapor extraction wells (VEP) in site 1.

		May 2021	**October 2021**	**December 2021**		
VEP	Depth m	^{222}Rn Bq m^{-3}	^{222}Rn Bq m^{-3}	^{222}Rn Bq m^{-3}	CH_4 ppm	VOCs ppm
VEP01	0–5	nm	nm	nm	0	0.4
	6–10	nm	nm	nm	0	151
	11–14	nm	nm	1100	60,000	615
	15–18	nm	nm	175,000	0	26
VEP04	0–5	56,000	70,000	nm	nm	nm
	6–10	nm	nm	nm	nm	nm
	11–14	nm	nm	nm	nm	nm
	15–18	127,000	113,000	nm	nm	nm

nm stans for not measured.

Total hydrocarbons were found in wells PZ02, PZ04, PZ09, PZ10, and PZ13 (Table A2); levels range from 50 µg L^{-1} (PZ09 in November 2020 and July 2021) to 137,280 µg L^{-1} (PZ13 in November 2020). The same wells were contaminated by MTBE, with concentration from 6 µg L^{-1} (PZ09 in November 2020) to 3295 µg L^{-1} (PZ02 in February 2020). ETBE was detected only in PZ02, PZ04, and PZ13; its levels ranged between 4 µg L^{-1} (PZ 02 in May 2021) and 1135 µg L^{-1} (PZ13 in February 2020). Other wells did not contain these substances in any sampling campaign.

During the study period, the average depth of the groundwater table was 17.73 m with a fluctuation of 0.15–0.20 m (Table A1). However, PZ10, PZ12, and occasionally PZ04 were affected by hydraulic highs as deep as 7 m below ground level due to water loss from adjacent municipal water pipelines.

4.2. Site 2

The radon activity concentrations in the groundwater extracted from site 2 wells in the period 2021–2022 are reported in Table 3. Tables A4 and A5 contain the groundwater levels and contents of NAPLs (total hydrocarbons, MTBE and ETBE), respectively. Radon concentrations ranged between 0.1 Bq L^{-1} (well PZ06 in February 2022) to 53 Bq L^{-1} (well SN03 in November 2021) (Figure 3). Two areas with average lower radon levels were recognized around wells PZ05 and PZ02 (2.2 Bq L^{-1}) and nearby wells PZ04, PZ06, PZ07, and PZ08 (1.6 Bq L^{-1}). On the other hand, higher average radon (12.4 Bq L^{-1}) was detected in wells located away from the contamination (wells PZ01, PZ09, SN1, SN3, and SN9).

Table 3. Radon activity concentrations in the 12 monitoring wells of site 2 in the period 2021–2022.

Wells	**^{222}Rn (Bq L^{-1})**	**^{222}Rn (Bq L^{-1})**	**^{222}Rn (Bq L^{-1})**	**^{222}Rn (Bq L^{-1})**	**^{222}Rn (Bq L^{-1})**	**^{222}Rn (Bq L^{-1})**
	May 2021	**September 2021**	**November 2021**	**February 2022**	**May 2022**	**September 2022**
SN01	10.1 ± 0.8	31.6 ± 2.2	25.1 ± 2.2	17.1 ± 1.3	-	-
PZ08	2.1 ± 0.3	2.4 ± 0.4	2.0 ± 1.6	1.9 ± 0.3	2.4 ± 0.4	1.6 ± 0.3
PZ09	10.4 ± 0.9	1.9 ± 0.3	5.1 ± 1.6	14.6 ± 1.2	4.3 ± 0.5	6.1 ± 0.6
SN09	22.5 ± 1.9	22.8 ± 1.7	30.9 ± 2.3	23.6 ± 1.7	-	-
SN03	47.1 ± 3.1	44.3 ± 3.0	53 ± 3.4	40.5 ± 2.7	-	-
PZ03	8.2 ± 0.8	31.2 ± 2.3	22.1 ± 1.9	13.4 ± 1.1	8.3 ± 0.8	9.6 ± 0.8
PZ05	2.6 ± 0.4	6.5 ± 0.6	3.3 ± 1.3	1.7 ± 0.3	1.6 ± 0.3	1.9 ± 0.3
PZ04	1.4 ± 0.3	4.9 ± 0.5	2.4 ± 1.5	1.8 0.3	10.3 ± 0.9	0.8 ± 0.2
PZ07	0.8 ± 0.2	1.5 ± 0.3	0.3 ± 1.5	1.3 ± 0.3	1.5 ± 0.3	1.1 ± 0.2
PZ02	0.9 ± 0.2	0.4 ± 0.2	-	0.3 ± 0.1	1.1 ± 0.2	1.0 ± 0.2
PZ06	0.8 ± 0.2	0.7 ± 0.2	0.6 ± 1.6	0.1 ± 0.1	1.4 ± 0.3	0.3 ± 0.1
PZ01	1.0 ± 0.2	3.0 ± 0.4	13.6 ± 1.7	1.2 0.2	10.9 ± 0.9	16.4 ± 1.2
SN01	10.1 ± 0.8	31.62.2	25.1 ± 2.2	17.1 ± 1.3	-	-

According to the radon deficit principle, wells PZ02 and PZ05 with low radon were characterized by the presence of total hydrocarbons (up to 26,000 μg L^{-1}) and to a lesser extent MTBE (up to 63 μg L^{-1}), whereas well PZ06 was affected only by moderate levels of MTBE (up to 54 μg L^{-1}). Finally, ETBE was always significantly found in well SN03 (up to 88 μg L^{-1}). It is worth noting that occasionally an oil film was found in wells PZ01, PZ02 (the closest to the contamination source), PZ04, PZ06, and PZ07, and high dissolved total hydrocarbons were detected in wells PZ01, PZ02, PZ03, PZ04, and PZ06 (September 2022).

The groundwater depth ranged from 3.37 m (well PZ01 in September 2021 and 2022) to 1.63 m (well PZ07 in November 2021) with relevant fluctuations and periodic change of flow direction influencing the location of the residual NAPLs.

5. Discussion

The groundwater radon concentrations in sites 1 and 2 were used to estimate average values for all monitoring wells over the study period. Radon data from clean wells of site 1 (those with higher radon levels and nearly no NAPLs, PZ03, PZ07, PZ14, PZ25, and PZ26) were averaged and used as a reference for calculating the radon deficit of dirty wells, as the ratio of the radon concentration in NAPL polluted aquifer and the equilibrium radon concentration in clean groundwater. The latter (119 ± 11 Bq L^{-1}) was compared and verified with a corresponding value ($^{222}Rn_{C,}$ 129 ± 10 Bq L^{-1}) calculated from the average ^{226}Ra specific activity of the Alban Hills Hydrogeological Unit (A_{Ra}, 85 Bq kg^{-1}, see Table 3), according to Equation (2), using a mineral density (r,) of 2.65 kg/L, a porosity (n) of 0.35, and an emanation radon efficiency (E) of 0.2 [23]:

$$^{222}Rn_C = A_{Ra} \times r \times E/n. \quad (2)$$

Since the two values agree within the error range, it was possible to determine with good approximation the NAPL saturation of contaminated wells in site 1 according to Equation (1) and show areas with higher saturation in a schematic map (Figure 5a). The well PZ13 and the adjacent area where the residual source zone is presumably located were characterized by the highest NAPL saturation (2.39%), while the wells located downgradient (PZ02, PZ04, PZ09, and PZ19) showed a saturation around or above 1%, apart from PZ19. PZ19 well was included in the plume zone, even if its saturation was much lower (0.42), because its apparent low saturation is calculated from a radon concentration affected by the proximity of PZ19 to a recharge well. Actually, the introduction of water treated with activated carbon filters absorb, not only the NAPLs, but also radon, which may not have time to reach the full equilibrium with its parent ^{226}Ra in the rock aquifer (low residence time).

Other wells surrounding the main plume or working as pumping wells were less polluted (PZ06, PZ8, PZ17, PZ18, and PZ19). The plume was elongated in the direction of the groundwater flow (NNW-ESE) and was perfectly retained in the fueling station area. Since the monitoring of the water table elevation and the groundwater quality was not continuous but periodical, it was difficult to demonstrate direct relationships between the rainfall distribution and the depth of the groundwater table on one side and the dissolved NAPL on the other. Using factorial analysis can help clarify these interactions.

Moreover, a recent study [22] carried out in a nearby area with a similar environmental and hydrogeological setting invoked a possible mechanism of contaminant (MTBE) remobilization from soil grains (mainly zeolites) linked to rainfall washing the terrain. Using the approach presented in [33], a dissipation half-life of 23 days was estimated for MTBE in the groundwater [22]. A similar process could be applied to site 1 where residual NAPLs, located at a depth of 6–12 m, could be removed, dissolved, transported, and affected by degradation and volatilization phenomena (natural attenuation).

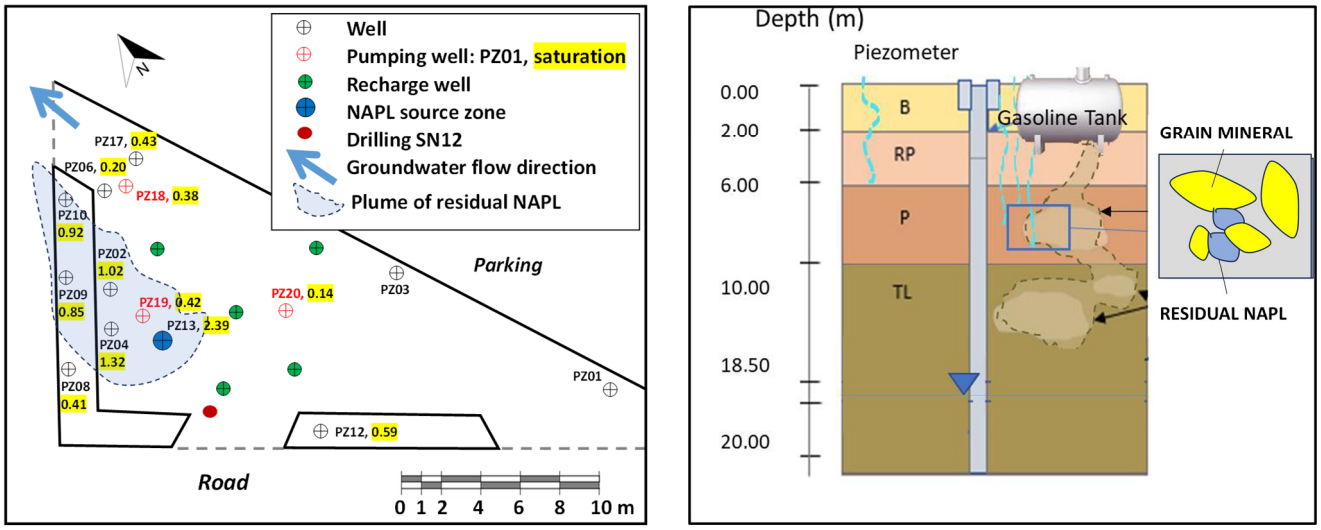

(**a**) (**b**)

Figure 5. Site 1. Schematic map of NAPL saturation in groundwater and plume reconstruction (**a**). Conceptual model of the contaminated area at well PZ13 (**b**). B is Backfill; RP stands for Reworked Pozzolan; P is Pozzolanelle Unit; TL1 is Tufo Lionato Unit (lithoid facies) and TL2 Tufo Lionato Unit (granular facies).

To assess and quantify these processes, principal component analysis was applied to the groundwater data of site 1, but not to the soil variables that were not available with the same frequency. The testing provided three main factors accounting for 85% of the total variance (Table 4). It is worth noting that the interpretation of factors is not always based on very high scores, but it is still supported by other descriptors.

Table 4. Factor analysis results in site 1. Variables are ^{222}Rn activity concentration (Bq L^{-1}), MTBE, ETBE, and total hydrocarbon concentrations (μg L^{-1}) in groundwater and groundwater table depth (m).

Variable	Factor 1	Factor 2	Factor 3
Radon	**−0.635**	0.007	**−0.740**
MTBE	**0.782**	0.056	**−0.431**
ETBE	**0.840**	−0.231	−0.153
Total hydrocarbons	**0.831**	−0.113	−0.003
Groundwater depth	−0.260	**−0.957**	0.007
Variance	2.4795	0.9859	0.7578
% Variance	49.6	19.7	15.2

Bold fonts highlight higher factor scores.

Factor 1 explaining the 50% of variance could be interpreted as the radon deficit process, which is the preferential solubility of radon in the NAPLs. A negative score of the groundwater depth (corresponding to a rainy period) was calculated with a negative value of radon and positive scores for MTBE, ETBE, and the total hydrocarbon concentrations. This implies that rainwater (and local leaks from municipal water pipelines) removed the residual NAPLs trapped in the aquifer pores, causing an increase in MTBE, ETBE, and the total hydrocarbon concentration in the groundwater where radon favorably dissolved with a reduction in the water radon contents. This process was already proposed in [23] for this site and [22] for a close fueling station in Roma.

Factor 2 accounted for a further 20% of variance (Table 4). Since a direct correlation was found between the depth of the groundwater and the concentrations of ETBE and total hydrocarbons, with approximately zero scores for radon and MTBE levels, we can

attribute this component to a degradation process of the first two substances in aerobic conditions. Precipitations (consistent with a reduction in the groundwater depth) introduced oxygen and nutrients into the aquifer promoting rapid biodegradation of ETBE and total hydrocarbons in the vadose zone, with reduced efficiency for MTBE [34,35]. The additions of biosurfactants (natural extracts of marine algae and plants) improved the separation and dispersion of hydrocarbon blobs, allowing the development and growth of natural microorganism that further degraded the NAPLs.

Factor 3 explained a supplementary 15% of variance (Table 4); it could be interpreted as volatilization of organic products (mainly MTBE) and radon degassing in the unsaturated part of the aquifer, also linked to the action of soil vapor extraction practices. MTBE is characterized by a higher vapor pressure and thus volatilizes more easily from the residual NAPL [36]. The low score of the groundwater table depth demonstrated no role of the small aquifer fluctuations.

NAPL saturation of polluted wells in site 2 was estimated according to Equation (1), based on the radon deficit values. The average radon level (17.1 Bq L^{-1}) of the groundwater extracted from PZ01, PZ09, SN01, SN03, and SN09 was used as a reference. The NAPL saturation in groundwater, represented on a schematic map (Figure 6a), ranged from about 8 to 54%, with the highest values in correspondence with the lower radon activity concentrations and stronger contamination. Such high saturations, compared with those calculated for site 1, are well explained by the recent age of this diesel spill.

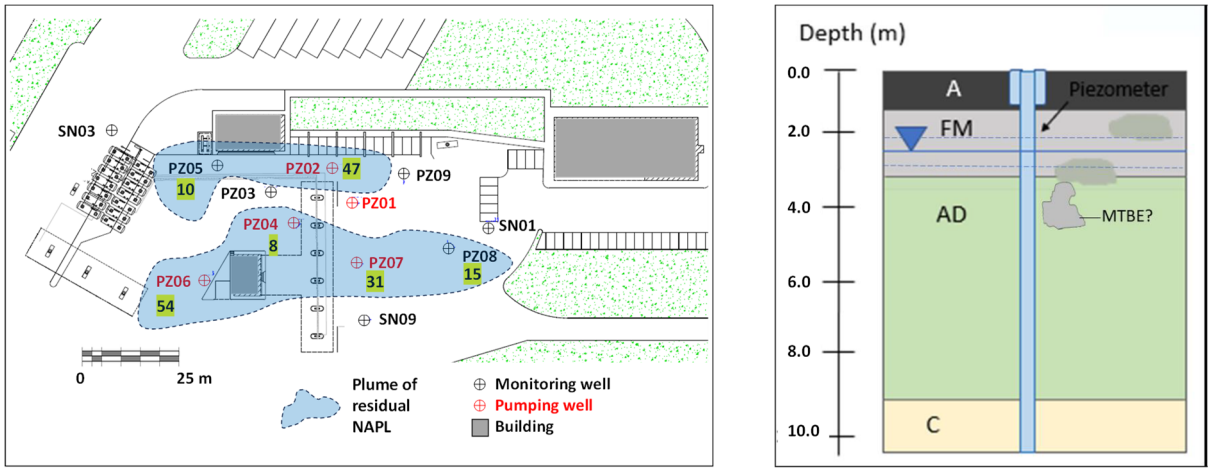

(**a**) (**b**)

Figure 6. Site 2. Schematic map of NAPL saturation in groundwater and plume reconstruction (**a**). Conceptual model of the contaminated area (**b**). A is asphalt; FM stands for filling material; AD is alluvial deposit; C is clay.

The presence of dissolved NAPLs was presumably associated with blobs of residual droplets of diesel and, to a lesser extent, gasoline in the soil pores that were mobilized by rainfall and groundwater table fluctuations. Their location was probably at a depth of 1–2 and 2–3 m below ground level, as suggested by traces of VOCs detected using a photoionization detector (PID) during the drilling of monitoring wells PZ02, PZ04, PZ06, and PZ07 in 2019, as notified by MARES. It is worth noting a good correspondence between higher NAPL saturation and the presence of soil VOCs.

The statistical analysis was also applied to the groundwater data of site 2, providing a different scenario (Table 5). The three main components accounted for 80% of the total variance. Factors 1, 2, and 3 explained about 37%, 23%, and 20% of variance, respectively. The first two components could be ascribed to the radon deficit process driven by rainfall (factor 1) and groundwater table fluctuations (factor 2) dynamics. Factor 3 could explain the biodegradation in anaerobic conditions.

Table 5. Factor analysis results in site 2. Variables are ^{222}Rn activity concentration (Bq L^{-1}), MTBE, ETBE, and total hydrocarbons concentrations (μg L^{-1}) in groundwater and groundwater table depth (m).

Variable	Factor 1	Factor 2	Factor 3
Radon	**0.953**	−0.014	−0.049
MTBE	0.219	**−0.512**	**−0.790**
ETBE	**0.872**	0.045	0.376
Total hydrocarbons	−0.128	**0.726**	−0.215
Groundwater depth	0.302	**0.590**	**−0.450**
Variance	1.8230	1.1391	1.0165
% Variance	36.5	22.8	20.3

Bold fonts highlight higher factor scores.

The interpretation of both factors 1 and 2 as a radon deficit process induced by the removal of the residual NAPLS was due to the shallow depth of the groundwater table (about 2 m) and its large annual fluctuations (up to 70 cm). In this case, it was possible to distinguish the contribution of rainfall that washed out the total hydrocarbons from the unsaturated zone and the effect of the groundwater table and the related capillary fringe on MTBE. Rainfall (factor 1) was effective with the total hydrocarbons related to the recent diesel spill and located at shallower depth where they were absorbed by backfill materials containing expanded clay, as demonstrated by the inverse correlation of the water table depth and radon concentration with the total hydrocarbons. The direct correlation of the groundwater depth with MTBE and ETBE contents suggests that these substances (linked to a previous gasoline spill) are located below the groundwater table and consequently are not removed by rainfall. In case of factor 2, the groundwater depth is inversely correlated with MTBE, consistent with the assumed location of residual MTBE at or just below the ground water surface. The direct correlation between the water table and total hydrocarbons strengthens the hypothesis that the total hydrocarbons are placed above and mobilized by rainfall. The absence of significant correlation with ETBE could be explained by its low degradation in anaerobic condition [37], No correlation with radon is evident, but this could be explained by the smoothing effect of the groundwater flow reversal on the transport and location of NAPLs and in turn on radon levels.

Factor 3 accounted for the biodegradation of MTBE and total hydrocarbons in anaerobic condition (Table 5). The negative score of the groundwater depth indicated that rainfall supplied oxygen and nutrients promoting the activity of microorganism on these compounds [36]. The reverse correlation with ETBE could be justified by a low degradation of ETBE in anaerobic conditions [37].

Based on these results, it was possible to develop the conceptual models of sites 1 (Figure 5b) and 2 (Figure 6b).

The residual NAPL source zone is located at well PZ13 (at a depth of 6 to 11 m) where the lowest radon and highest NAPL and VOC concentrations were detected (Figure 5), probably absorbed onto or trapped among mineral grains (for example zeolites [22,23]. Rainfall and, to a lesser extent, groundwater table fluctuations mobilize NAPLs that dissolve in the aquifer and are transported downstream, creating temporary plumes with a dissipation half-life of about 3 weeks [22,33]. The plume is perfectly confined in the fueling area by the mitigation system consisting of a series of pump-and-treat and vapor extraction wells. Radon deficit traces the NAPL location in the vadose and saturated parts of the aquifer due to its preferential solubility in organic phases; it accounts for about 50% of the variance in the groundwater data, as demonstrated by the principal component analysis. Average NAPL saturations, ranging from about 0.1 to 2.4%, are low, as expected by the age of the spill (about 20 years).

Phenomena of natural attenuation are actively working in the site; biodegradation of ETBE and total hydrocarbons in aerobic conditions justifies about 20% of variance, while volatilization of organic products, coupled with radon degassing, explains a further 15%. The use of biosurfactants certainly promoted the activity of natural microorganism and biodegradation.

Two areas of the residual NAPLs were recognized in site 2 around wells with lower radon and higher NAPL concentration (Figure 6). The presence of two single areas probably depends on the location and dynamics of the spills (gasoline first and diesel later) and on the change in the direction of the groundwater flow over the course of the year, as demonstrated in other areas [38]. In this site, the shallow depth of the groundwater table and its relevant fluctuations influence the mobilization of NAPLs more than in site 1, where rainfall mostly removed the residual contaminants. This hypothesis is supported by factorial analysis whose interpretation assigned 37% of the variance to rainfall (factor 1) and 23% (factor 2) to groundwater (and related capillary fringe). The radon deficit principle supported that and made it possible to calculate an average NAPL saturation of 8% to 54%, consistent with the younger age of the spills and the frequent presence of oil films in several wells. The residual NAPLs are probably located at a depth of 1–2 and 2–3 m, as confirmed by VOCs and it is plausible to expect MTBE blobs, and to a lesser extent residual ETBE, to be placed deeper than the total hydrocarbons due to the higher solubility of MTBE and the older age of the gasoline spill compared with the diesel release.

A comparison table is provided to summarize the main findings from the factorial analysis applied to sites 1 and 2. The interpretation of factors is not always based on very high scores, but it is still supported by other descriptors (Table 6).

Table 6. Comparison table with descriptors and driving factors (see factorial analysis) for site 1 and 2.

Descriptors	**Site 1**	**Site 2**
Groundwater depth (m)	−18	−2
Groundwater fluctuation (m)	0.15−0.20	0.70
Groundwater flow direction	constant	variable
Plume geometry	single plume	two plume areas
Depth of residual NAPLs (m)	−6/−10; −11/−14	−1/−2; −2/−3
Age of the spill (years)	20	3
Radon saturation	up to 2.4%	up to 54%
Aerobic/Anaerobic condition	Mostly aerobic	Mostly anaerobic
Mitigation	P and T; SVE; Biosurfactants	P and S
Driving Factors (% Variance)	**Site 1**	**Site 2**
Radon deficit promoted by rainfall	50	37
Radon deficit promoted by groundwater fluctuation	negligible	23
Degradation in aerobic condition	20	negligible
Degradation in anaerobic condition	negligible	20
Volatilization/degassing	15	negligible

P and T is Pump-and-Treat; SVE is Soil Vapor Extraction; P and S is Pump-and-Storage.

In site 1, rainfall more than water table fluctuation removes NAPLs from the tick vadose zone, producing the radon deficit. This is supported by the greater depth (about 18 m) of the groundwater table in site 1 and the location of the residual NAPLs in the vadose zone (at −6/−10 m and −11/−14 m), quite distant from the area of fluctuation of the piezometric level (Table 6). At site 2, relevant fluctuations (up to 0.7 m) of a shallow water table (about 2 m below ground level) contribute to mobilize the residual NAPLs (mainly MTBE) located next to the water table surface (at −1/−2 m and −2/−3 m), promoting the radon deficit. This is demonstrated by the variance attributed to these driving factors.

Degradation in aerobic conditions, rather than in anaerobic environment, occurs in site 1, coupled with stronger volatilization and degassing phenomena. These processes are coherent with a thick vadose zone. At site 2, the shallow depth and the dynamics of the water table makes the soil where the residual NAPLS are located more frequently anaerobic. Under these contrasting environmental conditions, the biodegradation in sites 1 and 2 proceed with different rates and mechanisms. The different loadings and correlations of NAPL concentrations, strengthened by appropriate references, help to outline these scenarios.

Finally, multivariate regression was applied to develop a model for radon estimation. Following, the equations were obtained for sites 1 and 2:

$$\text{Site1: Radon (Bq L}^{-1}) = 8.2 - 0.000485 \text{ Total Hydrocarbon (}\mu\text{g L}^{-1}) + 0.00440 \text{ MTBE (}\mu\text{g L}^{-1}) - 0.0495 \text{ ETBE (}\mu\text{g L}^{-1}) + 5.28 \text{ Groundwater depth (m)}$$

with R^2 = 22.48%, R^2 (adjusted) = 20.25%,

$$\text{Site 2: Radon (Bq L}^{-1}) = -6.85 - 0.000101 \text{ Total Hydrocarbon (}\mu\text{g L}^{-1}) + 0.01366 \text{ MTBE (}\mu\text{g L}^{-1}) + 0.4514 \text{ ETBE (}\mu\text{g L}^{-1}) + 5.15 \text{ Groundwater depth (m)}$$

with R^2 = 68.41%, R^2 (adjusted) = 66.23%,

Even if the regression coefficients, R^2, of both equations (22.48% for site 1 and 68.41% for site 2) are not very high, we want to stress the importance of this approach to estimate the value of an unknown variable starting from others or to establish relationships among factors. With a stronger dataset, the regression coefficients would be more robust and could help in predicting unavailable data and managing mitigation actions. To our knowledge, this is the first application of such a statistical approach to this type of dataset.

6. Conclusions

A radon deficit principle and approach were validated with a combined method consisting of multi-parameter monitoring (radon, NAPLs, and groundwater levels), chemical analysis, mapping, and statistical treatment (principal component analysis) in two sites of Roma with different geological and contamination settings.

Low radon in soil gas and groundwater made it possible to identify the location of the residual NAPLs. Groundwater table depth and fluctuations, location of residual NAPLs, and mitigation techniques were crucial for outlining the different relevance (relative weigh) of the radon deficit in the groundwater and that of the main natural and induced attenuation processes (degradation in aerobic and anaerobic environment and volatilization/degassing) in the two sites. Although factor analysis was applied only to the groundwater data, which were available more frequently in this case, and not to the soil, this statistical approach is relevant to both the saturated and unsaturated parts of an aquifer. Even if the interpretation of factors is not always based on very high scores due to the size of the dataset, it is still coherently supported by other descriptors, demonstrating the potential of this combined methodology.

Integrated conceptual models were outlined for the two sites, and inter-parametric regression models were proposed as a predictive tool in these areas and in others with similar features, to estimate the values of the unavailable variables and manage the remediation of polluted areas.

Author Contributions: Conceptualization, all authors; methodology, M.M., P.T., G.C. and M.S.; software, M.M. and G.C.; validation, all authors; formal analysis, M.M. and P.T.; investigation, all authors; resources, P.T., C.C. and E.R.; writing—original draft preparation, M.M. and P.T.; writing—review and editing, all authors; supervision, P.T., G.C. and M.S.; funding acquisition, P.T., C.C. and E.R. All authors have read and agreed to the published version of the manuscript.

Funding: PON "Ricerca e Innovazione" 2014–2020, Actions IV.4 e IV.5 "Dottorati su tematiche green". DM 1061/2021.

Institutional Review Board Statement: Not applicable.

Informed Consent Statement: Not applicable.

Data Availability Statement: The data presented in this study are available in article.

Acknowledgments: The authors wish to thank students who participated to this study: Emanuele Campo, Marika Mariani, and Manuela Portaro. A special acknowledgment is paid to Emiliano Montenero and another colleague for help in the field. We express our gratitude to Mares S.r.L. for accessing the sites and for sharing NAPL data with us. Antonio Francesco Amoruso, Federico Failla, and Daniele Lepore e Stella Lucifora of Mares contributed to sharing information and maintaining contacts between the study partners.

Conflicts of Interest: Authors Claudio Carusi and Elisa Rainaldi were employed by the company Mares S.r.L. The remaining authors declare that the research was conducted in the absence of any commercial or financial relationships that could be construed as a potential conflict of interest.

Appendix A

The appendix reports datasets that were not included in the main text. Tables A1 and A2 contain, respectively, the depth of the piezometric level and the concentration of NAPLs (total hydrocarbons, MTBE, and ETBE) in the 18 monitoring wells of site 1 in the period 2020–2022. ^{226}Ra specific activity of the seven subsamples collected from drilling SN12 in site 1 is included in Table A3.

Tables A4 and A5 report in this order the depth of the piezometric level and the contents of total hydrocarbons, MTBE, and ETBE at the 12 monitoring wells of site 2 in the period 2021–2022.

Table A1. Depth of the piezometric level at the 18 monitoring wells of site 1 in the period 2020–2022.

Wells	Depth (m)	Depth (m)	Depth (m)	Depth (m)	Depth (m)	Depth (m)	Depth (m)	Depth (m)
	February 2020	May 2020	November 2020	February 2021	May 2021	July 2021	November 2021	April 2022
PZ25	18.47	18.54	18.78	18.55	18.8	18.5	18.6	18.59
PZ26	17.26	17.34	17.59	17.35	17.65	17.3	17.4	17.37
PZ7	18.9	18.97	19.2	19.45	18.85	18.95	19.02	19.03
PZ14	19.38	19.47	19.7	18.98	19.36	19.4	19.53	19.50
PZ01	18.49	18.56	18.81	18.59	18.46	18.52	18.63	18.61
PZ03	18.83	18.9	19.14	18.92	18.78	18.85	18.97	18.94
PZ12	18.22	17.74	7.85	14.42	12.5	10.00	16.53	18.47
PZ17	18.09	18.78	19.02	18.77	18.65	18.72	18.82	18.78
PZ06	18.67	18.76	19.00	19.55	18.65	18.69	18.8	18.79
PZ10	7.09	9.2	9.22	15.35	15.05	17.03	16.3	18.00
PZ09	17.63	16.58	18.7	18.66	18.53	18.73	18.82	18.82
PZ08	18.65	18.74	18.99	18.77	18.65	18.74	18.83	18.81
PZ04	9.00	10.74	17.16	18.1	16.85	18.8	17.72	18.85
PZ02	18.67	18.75	18.97	18.78	18.67	18.73	18.8	18.82
PZ13	18.64	18.66	18.63	18.48	18.4	18.47	18.65	19.00

Table A2. Contents total hydrocarbons (T), MTBE (M) and ETBE (E), all in micrograms L^{-1}, in the 18 wells of site 1 in the period 2020–2022.

Well	T	M	E	T	M	E	T	M	E	T	M	E	T	M	E	T	M	E	T	M	E	T	M	E
	February 2020			**May 2020**			**November 2020**			**February 2021**			**May 2021**			**July 2021**			**November 2021**			**April 2022**		
PZ25	<20	<1	<1	<20	<1	<1	<20	<1	<1	<20	<1	<1	<20	<1	<1	<30	<1	<1	<30	<1	<1	<30	<1	<1
PZ26	<20	<1	<1	<20	<1	<1	<20	<1	<1	<20	<1	<1	<20	<1	<1	<30	<1	<1	<30	<1	<1	<30	<1	<1
PZ7	<20	<1	<1	<20	<1	<1	<20	<1	<1	<20	<1	<1	<20	<1	<1	<30	<1	<1	<30	<1	<1	<30	<1	<1
PZ14	<20	15	12	<20	21	17	<20	6	4	35	2	1	<20	2	1	<30	2	1	<30	7	1	<30	2	2
PZ01	<20	<1	<1	<20	<1	<1	<20	<1	<1	<20	<1	<1	<20	<1	<1	<20	14	5	<20	<1	<1	<30	<1	<1
PZ03	<20	<1	<1	<20	<1	<1	<20	<1	<1	<20	<1	<1	<20	2	<1	<30	2	1	<30	<1	<1	<30	2	2
PZ12	<20	<1	<1	<20	<1	<1	<20	6	6	210	<1	3	<20	<1	<1	<30	1	<1	<30	1	<1	<30	<1	<1
PZ17	<20	<1	4	<20	7	6	<20	<1	<1	<20	<1	<1	<20	<1	<1	<30	<1	<1	<30	<1	<1	<30	<1	<1
PZ06	<20	2	<1	<20	6	1	<20	6	<1	<20	3	<1	<20	2	<1	<30	14	4	<30	4	<1	<30	1	1
PZ10	70	**129**	19	**7515**	<1	31	**33,490**	**124**	21	**28,360**	**124**	22	**43,705**	<1	<1	**7000**	**77**	24	**9500**	**255**	30	**8600**	**47**	**47**
PZ09	<20	10	2	100	**106**	38	50	6	<1	**5160**	<1	17	**1695**	**66**	18	50	59	9	75	**159**	13	<30	5	5
PZ08	<20	<1	<1	60	1	<1	<20	8	2	<20	<1	<1	<20	<1	<1	75	<1	<1	<30	<1	<1	<30	<1	<1
PZ04	80	**404**	**59**	**720**	**580**	**141**	445	160	93	**990**	**47**	**43**	**3075**	**155**	**87**	**2980**	**216**	**54**	<30	**346**	**580**	<30	29	29
PZ02	**43,235**	**3295**	**108**	**48,020**	**1180**	**112**	**56,845**	**143**	**83**	**31,535**	<1	<1	**5540**	**66**	4	**2500**	**90**	16	**7000**	**159**	**275**	56	8.5	8.5
PZ13	**89,155**	**2710**	**1335**	**55,350**	**767**	**525**	**137,280**	**470**	**422**	**91,950**	**286**	**374**	**93,410**	**402**	**391**	**40,000**	**166**	470	**5000**	**431**	**500**	**9600**	**225**	**225**

Detection limit for TH, MTBE and ETBE determination are 20, 1 and 1 micrograms L^{-1}, respectively. Values in bold are those which exceed Italian reference level of 350, 40, 40 micrograms L^{-1} for total hydrocarbons, MTBE and ETBE, respectively.

Table A3. ^{226}Ra specific activity of seven subsamples collected from drilling 12 (site 1). See Figures 2 and 4 for location.

Sample	Depth Below Ground Level	^{226}Ra Specific Activity
	(m)	(Bq kg^{-1})
SN 12 a	6–7	133 ± 7
SN 12 b	7–8	55 ± 3
SN 12 c	9–10	52 ± 3
SN 12 d	12–13	37 ± 2
SN 12 e	14–15	53 ± 3
SN 12 f	16–17	108 ± 5
SN 12 g	19–20	157 ± 8

Table A4. Depth of the piezometric level at the monitoring wells of site 2 in the period 2021–2022.

Wells	Depth (m)	Depth (m)	Depth (m)	Depth (m)	Depth (m)	Depth (m)
	May 2021	September 2021	November 2021	February 2022	May 2022	September 2022
SN01	1.96	2.84	2.65	2.03	n.a.	n.a.
PZ08	1.66	1.98	1.92	1.75	1.78	1.91
PZ09	2.16	2.63	2.72	2.22	2.12	n.a.
SN09	2.12	2.89	2.62	2.17	n.a.	n.a.
SN03	2.10	2.74	2.51	2.16	n.a.	n.a.
PZ03	2.14	3.07	2.74	2.23	2.30	2.77
PZ05	2.20	2.47	2.40	2.27	2.30	2.41
PZ04	2.30	3.80	1.87	2.08	2.11	4.50
PZ07	1.80	2.10	1.63	2.05	1.89	1.98
PZ02	2.02	2.33	1.91	1.87	2.11	2.23
PZ06	1.81	2.13	1.69	2.08	1.90	2.00
SN01	1.93	3.37	1.84	1.89	2.22	3.37

n.a. stands for not available.

Table A5. Contents total hydrocarbons (T), MTBE (M) and ETBE (E), all in μg L^{-1}, in the 12 wells of site 2 in the period 2021–2022.

Wells	T	M	E	T	M	E	T	M	E	T	M	E	T	M	E	T	M	E
	May 2021			September 2021			November 2021			February 2022			May 2022			September 2022		
SN01	<30	<1	<1	<30	<1	<1	<30	4,4	<1	<30	<1	<1	na	na	na	na	na	na
PZ08	<30	16	<1	<30	<1	<1	<30	1.8	<1	<30	6	<1	15	0.5	0.5	90	1.3	0.5
PZ09	<30	11	<1	<30	<1	<1	62	9.6	<1	<30	10	<1	15	1.6	0.5	15	1.2	0.5
SN09	<30	**120**	<1	<30	**43**	<1	<30	**156**	<1	<30	**69**	<1	na	na	na	na	na	na
SN03	<30	2.1	**91**	<30	3.5	**78**	<30	12	**105**	<30	2	78	na	na	na	na	na	na
PZ03	<30	2.3	<1	<30	4	4	<30	10	7	<30	2	1.7	15	0.5	0.5	**4600**	2.7	1.5
PZ05	<30	3.9	9.5	<30	1	1.7	<30	3	3	<30	**63**	6	240	1.5	0.5	90	11	2
PZ04	<30	2.7	<1	<30	3	2.6	<30	18	5	<30	<1	<1	15	1.3	0.5	**1300**	0.5	0.5
PZ07	<30	<1	<1	<30	3	3	<30	5	1.4	<30	5	<1	na	na	na	na	na	na
PZ02	<30	<1	<1	<30	<1	<1	180	4	<1	<30	<1	<1	na	na	na	**26,000**	1.2	0.5
PZ06	<30	<1	<1	<30	**54**	2.7	<30	19	<1	<30	<1	<1	**1120**	2.5	0.5	**1300**	10	1
PZ01	<30	28.6	<1	<30	7.6	2	<30	36	1.36	<30	<1	<1	15	2.3	0.5	**9400**	2.4	0.5

Detection limit for total hydrocarbons, MTBE and ETBE determination are 20, 1, and 1 μg L^{-1}, respectively. na stands for not available. Values in bold are those which exceed Italian reference level of 350, 40 and 40 μg L^{-1} for total hydrocarbons, MTBE and ETBE, respectively.

References

1. McLaughlan, R.G.; Merrick, N.P.; Davis, G.B. Natural attenuation: A scoping review. In *CRC for Contamination Assessment and Remediation of the Environment*; Technical Report Series 3; CRC CARE: Callaghan, NSW, Australia, 2006; pp. 1–65.
2. Illman, W.A.; Alvarez, P.J. Performance Assessment of Bioremediation and Natural Attenuation. *Crit. Rev. Environ. Sci. Technol.* **2009**, *39*, 209–270. [CrossRef]
3. Braeckevelt, M.; Fischer, A.; Kästner, M. Field applicability of Compound-Specific Isotope Analysis (CSIA) for characterization and quantification of in situ contaminant degradation in aquifers. *Appl. Microbiol. Biotechnol.* **2012**, *94*, 1401–1421. [CrossRef] [PubMed]
4. Essaid, H.I.; Bekins, B.A.; Herkelrath, W.N.; Delin, G.N. Crude Oil at the Bemidji Site: 25 Years of Monitoring, Modeling, and Understanding. *Groundwater* **2009**, *49*, 706–726. [CrossRef] [PubMed]
5. Barrio-Parra, F.; Izquierdo-Díaz, M.; Díaz-Curiel, J.; De Miguel, E. Field performance of the radon-deficit technique to detect and delineate a complex DNAPL accumulation in a multi-layer soil profile. *Environ. Pollut.* **2021**, *269*, 116200. [CrossRef] [PubMed]
6. Weiss, R.F. *Krypton, Xenon and Radon Gas-Solubilities, Fluid Phase Equilibria*; Pergamon Press: Oxford, UK, 1980.
7. Hunkeler, D.; Hoehn, E.; Hohener, P.; Zeyer, J. 222 Rn as a Partitioning Tracer to Detect Diesel Fuel Contamination in Aquifers: Laboratory Study and Field Observations. *Environ. Sci. Technol.* **1997**, *31*, 3180–3187. [CrossRef]
8. Semprini, L.; Hopkins, O.S.; Tasker, B.R. Laboratory, Field, and Modeling Studies of Radon-222 as a Natural Tracer for Monitoring NAPL Contamination. *Transp. Porous Media* **2000**, *38*, 223–240. [CrossRef]
9. Schubert, M.; Freyer, K.; Treutler, H.C.; Weib, H. Using the soil gas radon as an indicator for ground contaminanion by non-aqueous phase-liquids. *J. Soils Sediments* **2001**, *4*, 217–222. [CrossRef]
10. Schubert, M.; Freyer, K.; Treutler, H.C.; Weiss, H. Using radon-222 in soil gas as an indicator of subsurface contamination by non-aqueous phase-liquid (NAPLs). *Geofis. Int.* **2002**, *41*, 433–437.
11. Höhener, P.; Surbeck, H. Radon-222 as a Tracer for Nonaqueous Phase Liquid in the Vadose Zone: Experiments and Analytical Model. *Vadose Zone J.* **2004**, *3*, 1276. [CrossRef]
12. Schubert, M.; Peña, P.; Balcázar, M.; Meissner, R.; Lopez, A.; Flores, J.H. Determination of radon distribution patterns in the upper soil as a tool for the localization of subsurface NAPL contamination. *Radiat. Meas.* **2005**, *40*, 633–637. [CrossRef]
13. Schubert, M.; Paschke, A.; Lau, S.; Geyer, W.; Knoller, K. Radon as a naturally occurring tracer for the assessment of residual NAPL contamination of aquifers. *Environ. Pollut.* **2007**, *145*, 920–927. [CrossRef]
14. Garcia-Gonzalez, J.E.; Ortega, M.F.; Chacon, E.; Mazadiego, L.F.; Miguel, E.D. Field validation of radon monitoring as a screening methodology for NAPL-contaminated sites. *Appl. Geochem.* **2008**, *23*, 2753–2758. [CrossRef]
15. Barbosa, E.Q.Q.; Galhardi, J.A.; Bonotto, D.M.M. The use of radon (Rn-222) and volatile organic compounds in monitoring soil gas to localize NAPL contamination at a gas station in Rio Claro, Sao Paulo State, Brazil. *Radiat. Meas.* **2014**, *66*, 1–4. [CrossRef]
16. De Simone, G.; Galli, G.; Lucchetti, C.; Tuccimei, P. Using Natural Radon as a Tracer of Gasoline Contamination. *Procedia Earth Planet. Sci.* **2015**, *13*, 104–107. [CrossRef]
17. Schubert, M. Using radon as environmental tracer for the assessment of subsurface Non-Aqueous Phase Liquid (NAPL) contamination—A review. *Eur. Phys. J. Spec. Top.* **2015**, *224*, 717–730. [CrossRef]
18. De Simone, G.; Lucchetti, C.; Pompilj, F.; Galli, G.; Tuccimei, P.; Curatolo, P.; Giorgi, R. Soil radon survey to assess NAPL contamination from an ancient spill. Do kerosene vapors affect radon partition? *J. Environ. Radioact.* **2017**, *171*, 138–147. [CrossRef]
19. De Simone, G.; Lucchetti, C.; Pompilj, F.; Galli, G.; Tuccimei, P. Laboratory simulation of recent NAPL spills to investigate radon partition among NAPL vapours and soil air. *Appl. Radiat. Isot.* **2017**, *120*, 106–110. [CrossRef]
20. Castelluccio, M.; Agrahari, S.; De Simone, G.; Pompilj, F.; Lucchetti, C.; Sengupta, D.; Galli, G.; Friello, P.; Curatolo, P.; Giorgi, R.; et al. Using a multi-method approach based on soil radon deficit, resistivity, and induced polarization measurements tomonitor non-aqueous phase liquid contamination in two study areas in Italy and India. *Environ. Sci. Pollut. Res.* **2018**, *25*, 12515–12527. [CrossRef]
21. De Miguel, E.; Barrio-Parra, F.; Elio, J.; Izquierdo-Diaz, M.; Fernandez, J.; Garcia-Gonzalez, J.E.; Mazadiego, L.F.; Medina, R. Applicability of radon emanometry in lithologically discontinuous sites contaminated by organic chemicals. *Environ. Sci. Pollut. Res.* **2018**, *25*, 20255–20263. [CrossRef]
22. Briganti, A.; Tuccimei, P.; Voltaggio, M.; Carusi, C.; Castelluccio, M.; Galli, G.; Lucchetti, C.; Soligo, M. Assessing MTBE residual contamination in groundwater using radon. *Appl. Geochem.* **2020**, *116*, 104583. [CrossRef]
23. Mattia, M.; Tuccimei, P.; Soligo, M.; Carusi, C.; Rainaldi, E.; Amoruso, A.F.; Lepore, D. Radon as a natural tracer for monitoring NAPL groundwater contamination. *Water* **2020**, *12*, 3327. [CrossRef]
24. Karapanagioti, H.K.; Gaganis, P.; Burganos, V.N. Modeling attenuation of volatile organic mixtures in the unsaturated zone: Codes and usage. *Environ. Model. Softw.* **2003**, *18*, 329–337. [CrossRef]
25. Ponsin, V.; Chablais, A.; Dumont, J.; Radakovitch, O.; Höhener, P. ^{222}Rn as Natural Tracer for LNAPL Recovery in a Crude Oil-Contaminated Aquifer. *Groundw. Monit. Remediat.* **2015**, *35*, 30–38. [CrossRef]
26. Mazza, R.; La Vigna, F.; Capelli, G.; Dimasi, M.; Mancini, M.; Mastrorillo, L. Idrogeologia del territorio di Roma. *Acque Sotter. Ital. J. Groundw.* **2016**, *4*, 19–30.

27. Briganti, A.; Voltaggio, M.; Tuccimei, P.; Soligo, M.; Rainaldi, E.; Carusi, C. Radiometric dating of Light Non-Aqueous Phase Liquids (LNAPLs) dispersed in soil: A low environmental impact tool for natural resource restorations and protection. *Appl. Geochem.* **2023**, *159*, 105817. [CrossRef]
28. De Simone, G.; Lucchetti, C.; Galli, G.; Tuccimei, P. Correcting for H_2O interference using a RAD7 electrostatic collection based silicon detector. *J. Environ. Radioact.* **2016**, *162–163*, 146–153. [CrossRef]
29. Lucchetti, C.; De Simone, G.; Galli, G.; Tuccimei, P. Evaluating radon loss from water during storage in standard PET, bio-based PET, and PLA bottles. *Radiat. Meas.* **2016**, *84*, 1–8. [CrossRef]
30. Tuccimei, P.; Lane-Smith, D.; Galli, G.; Simko, J.; Cook, I.; Bond, C.E.; Lucchetti, C.; De Simone, G. Our PET project: An unlimited supply of big and small water sample vials for the assay of radon in water. *J. Radioanal. Nucl. Chem.* **2016**, *307*, 2277–2280. [CrossRef]
31. De Simone, G.; Galli, G.; Lucchetti, C.; Tuccimei, P. Calibration of Big Bottle RAD H_2O set-up for radon in water using HDPE bottles. *Radiat. Meas.* **2015**, *76*, 1–7. [CrossRef]
32. Giustini, F.; Ruggiero, L.; Sciarra, A.; Beaubien, S.E.; Graziani, S.; Galli, G.; Pizzino, L.; Tartarello, M.C.; Lucchetti, C.; Sirianni, P.; et al. Measurements of indoor gamma dose rate in buildings: New data from a volcanic area of central Italy. *Int. J. Environ. Res. Public Health* **2022**, *19*, 666. [CrossRef]
33. Metcalf, M.J.; Stevens, G.J.; Robbins, G.A. Application of first order kinetics to characterize MTBE natural attenuation in groundwater. *J. Contam. Hydrol.* **2016**, *187*, 47–54. [CrossRef] [PubMed]
34. Kharoune, M.; Kharoune, L.; Lebault, J.-M.; Pauss, A. Aerobic degradation of ethyl-tert-butyl ether by a microbial consortium: Selection and evaluation of biodegradation ability. *Environ. Toxicol. Chem.* **2002**, *21*, 2052–2058. [PubMed]
35. Thornton, S.F.; Nicholls, H.C.G.; Rolfe, S.A.; Mallinson, H.E.H.; Spence, N.J. Biodegradation and fate of ethyl-tert-butyl ether (ETBE) in soil and groudwater: A review. *J. Hazard. Mater.* **2020**, *391*, 122046. [CrossRef] [PubMed]
36. Ma, J.; Xiong, D.; Li, H.; Ding, Y.; Xia, X.; Yang, Y. Vapor intrusion risk of fuel ether oxygenates methyl tert-butyl ether (MTBE), tert-amyl methyl ether (TAME) and ethyl tert-butyl ether (ETBE): A modeling study. *J. Hazard. Mater.* **2017**, *332*, 10–18. [CrossRef]
37. van der Waals, M.J.; Pijls, C.; Sinke, A.J.C.; Langenhoff, A.A.M.; Smidt, H.; Gerritse, J. Anaerobic degradation of a mixture of MtBE, EtBE, TBA and benzene under different redox conditions. *Appl. Microbiol. Biotechnol.* **2018**, *102*, 3387–3397. [CrossRef]
38. Bjerg, P.L.; Albrechtsen, H.-J.; Kjeldsen, P.; Christensen, T.H.; Cozzarelli, I. The Groundwater Geochemistry of Waste Disposal Facilities. In *Treatise on Geochemistry*; Davis, A.M., Holland, H.D., Turekian, K.K., Eds.; Elsevier: Pergamon, Turkey, 2003; Volume 9, Issue 16; pp. 578–612.